ACS APPLIED MATERIALS & INTERFACES

www.acsami.org

Research Article

Zinc-Embedded Polyamide Fabrics Inactivate SARS-CoV-2 and Influenza A Virus

Vikram Gopal,* Benjamin E. Nilsson-Payant, Hollie French, Jurre Y. Siegers, Wai-shing Yung, Matthew Hardwick, and Aartjan J. W. te Velthuis*

Cite This: *ACS Appl. Mater. Interfaces* 2021, 13, 30317−30325

Read Online

ACCESS | Metrics & More | Article Recommendations

ABSTRACT: Influenza A viruses (IAV) and SARS-CoV-2 can spread via liquid droplets and aerosols. Face masks and other personal protective equipment (PPE) can act as barriers that prevent the spread of these viruses. However, IAV and SARS-CoV-2 are stable for hours on various materials, which makes frequent and correct disposal of these PPE important. Metal ions embedded into PPE may inactivate respiratory viruses, but confounding factors such as adsorption of viruses make measuring and optimizing the inactivation characteristics difficult. Here, we used polyamide 6.6 (PA66) fibers containing embedded zinc ions and systematically investigated if these fibers can adsorb and inactivate SARS-CoV-2 and IAV H1N1 when woven into a fabric. We found that our PA66-based fabric decreased the IAV H1N1 and SARS-CoV-2 titer by approximately 100-fold. Moreover, we found that the zinc content and the virus inactivating property of the fabric remained stable over 50 standardized washes. Overall, these results provide insights into the development of reusable PPE that offer protection against RNA virus spread.

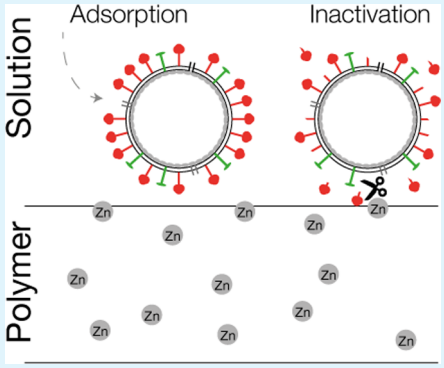

KEYWORDS: *influenza, coronavirus, absorption, zinc, face mask*

INTRODUCTION

Infections with influenza A viruses (IAV), influenza B viruses, and coronaviruses (CoV) are a burden on our healthcare systems and economy. These respiratory RNA viruses transmit through aerosols, liquid droplets, and fomites and typically cause a mild disease with symptoms including nasopharyngitis, fever, coughing, and headache. In addition, IAV and CoV strains can cause pandemics with even graver death tolls and economic consequences. The most recent example is the SARS-CoV-2 pandemic strain, the causative agent of CoV Disease 2019 (COVID-19).[1] Understanding how we can efficiently prevent the spread of these viruses will be important for current and future RNA virus outbreaks.

An IAV particle consists of a double-layered membrane in which multiple copies of the viral hemagglutinin (HA), matrix 2 (M2), and neuraminidase (NA) proteins are embedded.[2] The viral RNA genome resides inside the membrane and consists of eight negative-sense single-stranded RNA segments that are encapsidated by the viral nucleoprotein (NP) and RNA polymerase as ribonucleoprotein (RNP) complexes.[3] The SARS-CoV-2 virion consists of a double-layered membrane and the membrane proteins spike (S), envelope (E), and matrix (M). In contrast to IAV, the SARS-CoV-2 genome is a non-segmented positive-sense RNA that is bound by the viral nucleocapsid protein (N).[4,5] Infection of a host cell requires binding of the SARS-CoV-2 S protein to the cellular receptor ACE2, while IAV uses its HA protein to bind sialic acid receptors.[6]

While antivirals and vaccines are available for the treatment and containment of IAV and SARS-CoV-2 infections,[7−10] the approaches may not be effective against future emerging strains.[11,12] The use of personal protective equipment (PPE), such as face masks, is therefore recommended to reduce the spread of novel respiratory viruses.[13−15] However, PPE require careful decontamination to allow their re-use because respiratory viruses are stable for days to hours on fabrics.[16−21] Development of PPE that can trap and inactivate respiratory viruses may help address some of these concerns.

Previous research has shown that IAV and CoV can be inactivated by silver nanoparticles, copper nanoparticles, cuprous oxide (Cu_2O) or cupric oxide (CuO) spays, and copper or zinc surfaces or fibers.[22−28] While the underlying inactivation mechanisms are not fully understood, evidence suggests that metal ions can induce RNA hydrolysis, membrane destabilization, or viral protein inactivation and

Received: March 8, 2021
Accepted: June 17, 2021
Published: June 27, 2021

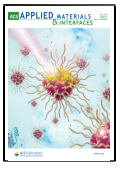

degradation.[29−31] So far, few studies have investigated if metal ions embedded in fabrics can inactivate RNA viruses, in part because absorbance and fabric density differences present confounding factors that inactivation protocols do not account for.

We here show how we can remove IAV H1N1 and pandemic SARS-CoV-2 from a woven PA66 fabric to measure the number of remaining active viruses. Using this advancement, we find that a zinc-containing PA66-based fabric decreased the IAV H1N1 and pandemic SARS-CoV-2 titer by approximately 2-logs. This reduction is more than sufficient to inactivate the number of infectious IAV particles (∼24 plaque-forming units [pfu]) present in a cough.[32] Overall, these results provide new insights into the development of testing protocols for "pathogen-free" fabrics.

RESULTS

Influenza Virus Adsorbance by Cotton, Polypropylene, and Polyamide. Fabrics vary by their filtration properties, breathability, hydrophobicity, electrostaticity, and/or weight per square meter (gram/m^2). In addition, fabrics can have different moisture retention abilities depending on environmental conditions.[33] These different properties affect how fabrics trap and/or release aerosols or liquid droplets containing respiratory RNA viruses. Presently, it is not fully understood how moisture retention is correlated with virus particle adsorption. To investigate this relationship, we added IAV strain A/WSN/33 (H1N1) to International Antimicrobial Council (IAC) issued cotton, a textile PA66 fabric, or polypropylene (PPP) from a disposable type II 3-ply face mask (Figure 1A). After a 30 min of incubation at room temperature, the fabrics were washed with phosphate-buffered saline (PBS) to remove virus that had not been adsorbed (Figure 1B). To estimate the amount of remaining liquid on each fabric, each sample tube with fabric was weighed and compared to its dry weight. As shown in Figure 1C,D, cotton and PA66 retained more liquid than PPP, both relative to the applied volume and the weight of the fabric. Subsequent analysis of the IAV titer in the input and fabric washes showed that the cotton and woven PA66 fabrics readily adsorbed the applied virus, while less virus was adsorbed by the PPP fabric (Figure 1E,F), which is in line with the higher hydrophobicity of PPP relative to PA66 and cotton.[34]

To remove IAV from the cotton and PA66 fabrics without inactivating the virus, we added different concentrations of polysorbate-80 (tween-80)—a mild detergent that is also used in IAV vaccine preparations—to the PBS wash buffer (Figure 1G). We did not observe any cytopathic effects of the detergent on the Madin−Darby Canine Kidney (MDCK) cells when diluted in MEM for plaque assays. Interestingly, we did find that the presence of 0.05−0.1% tween-80 increased the apparent viral titer relative to infections in PBS (Figure 1G), whereas 0.25−0.5% tween-80 reduced the apparent IAV plaque size (Figure 1G). In addition, we found that 0.05% tween-80 in PBS succeeded in recovering more than 94% of the virus from the PA66 woven fabric, whereas 61% was removed from the cotton fabric (Figure 1H,I). No virus plaques were recovered when we used 1% or higher concentrations of tween-80, likely because tween-80 destabilized the membrane or membrane-embedded glycoproteins of the virus particles (Figure 1I).

We next measured if SARS-CoV-2 could be removed from cotton and woven PA66 and found that over 92% of SARS-CoV-2 can be recovered from the woven PA66 fabric using 0.05% tween-80, while up to 59% could be recovered from the cotton fabric (Figure 1J). Together, these results demonstrate that IAV and SARS-CoV-2 in liquid suspension are strongly adsorbed by cotton and PA66, suggesting that these materials would trap respiratory viruses inside face masks. At the same time, these findings imply that PPP is poor at trapping

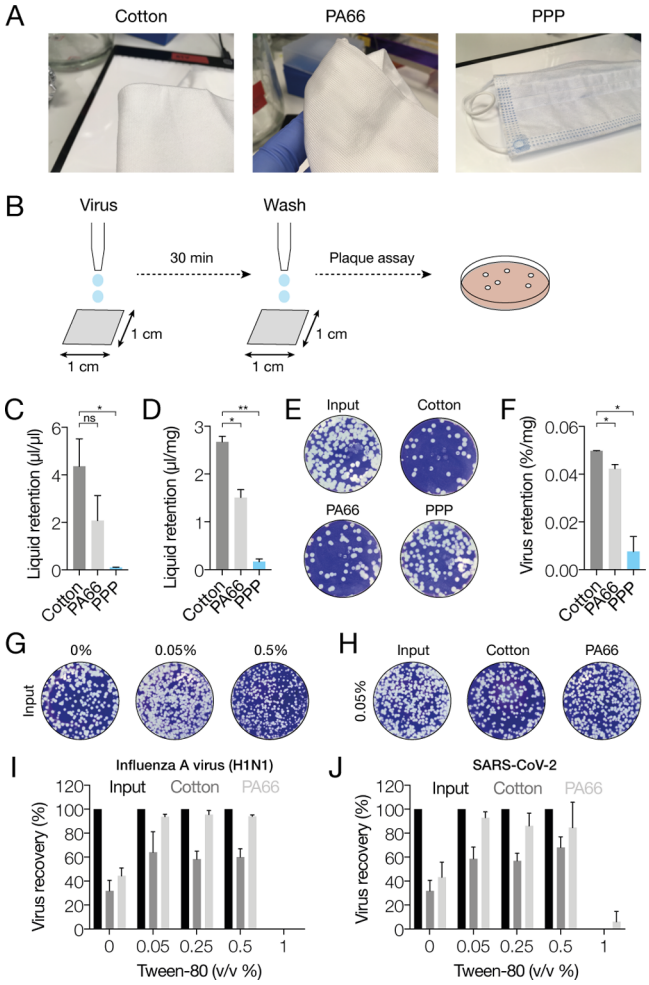

Figure 1. Adsorption and release of IAV and SARS-CoV-2 from fabrics. (A) Photographs of cotton control, PA66, and PPP fabric samples. (B) Schematic of experimental procedure for exposing and isolating RNA virus from fabrics. (C) Analysis of virus medium retention by fabrics per volume of input medium. Values were obtained by weighing each fabric before and after addition of virus medium and after removal of the virus medium. (D) Analysis of virus medium retention by fabrics normalized by dry weight of each fabric. Values were obtained by weighing each fabric before and after addition of virus medium and after removal of the virus medium. (E) Plaque assay of IAV present in virus medium after removal of the medium from each fabric. (F) Quantitation of the amount of virus remaining on each fabric, normalized by the dry weight of each fabric. (G) Effect of different tween-80 concentrations on IAV plaque assay read-out. (H) Effect of 0.05% tween-80 in PBS on the amount of virus released from each fabric. (I) Quantitation of IAV titers after adsorption of the virus to the fabrics and washing of the fabrics with PBS or PBS containing different concentrations of tween-80. (J) Quantitation of SARS-CoV-2 titers after adsorption of the virus to the fabrics and washing of the fabrics with PBS or PBS containing different concentrations of tween-80. Error bars indicate standard deviation. Asterisk indicates p-value, with $*p < 0.05$, $**p < 0.005$, and ns $p > 0.05$.

https://doi.org/10.1021/acsami.1c04412
ACS Appl. Mater. Interfaces 2021, 13, 30317−30325

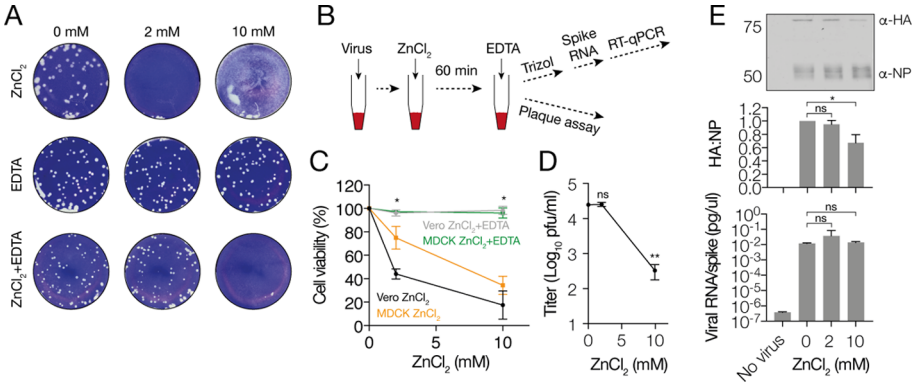

Figure 2. IAV is inactivated by zinc ions. (A) Plaque assay showing the effect of different zinc chloride and EDTA concentrations on IAV titers. (B) Experimental approach for inactivating IAV with zinc ions and neutralization of zinc ions using EDTA. (C) Cytotoxicity analysis of zinc chloride and EDTA in MDCK cells. (D) IAV titers after exposure to zinc chloride and neutralization with EDTA as measured on MDCK and Vero E6 cells. (E) Western blot IAV HA and NP protein levels after exposure to zinc chloride and neutralization with EDTA. The upper panel shows quantitation of western signal and the middle panel shows the western signal as detected with LI-COR. The bottom panel shows NA segment RT-qPCR analysis of IAV after exposure to zinc chloride and neutralization with EDTA. Error bars represent standard deviation. Asterisk indicates p-value, with $*p < 0.05$, $**p < 0.005$, and ns $p > 0.05$.

respiratory viruses. Since IAV and SARS-CoV-2 can be removed from a PA66 fabric with a mild detergent, this protocol can be useful for testing the inactivating properties of fabrics.

Influenza Virus Is Inactivated by Zinc Ions. Copper and zinc surfaces or particles can inactivate IAV strains, SARS-CoV-2, and seasonal CoV HCoV-229E, and PPP imbued with copper oxide can inactivate IAV.[22,25,26,29,30,35] As an embedded component of a polymer, zinc may provide at least three benefits over copper. First, zinc has a much higher propensity to ionize than copper, thereby providing a much faster reaction potential. Second, zinc oxide is considered a Generally regarded as Safe (GRAS) compound by the FDA, which can speed up the development process. Third, zinc does not cause discoloration of the polymer or fabric, enabling a broader applicability. However, like copper, zinc ions are cytotoxic in tissue culture (Figure 2A), which confounds analysis of their effect on viral titers. We found that addition of an equimolar concentration of EDTA following the virus incubation with zinc ions (Figure 2B) can efficiently chelate zinc ions and prevent cytotoxic effects (Figure 2C). EDTA alone does not have any cytotoxic effects when diluted in a plaque assay and it does not reduce viral titers (Figure 2A).

To investigate if zinc ions can directly inactivate IAV, we incubated influenza virus with varying concentrations of zinc chloride. After 60 min, the reactions were stopped with an equimolar amount of EDTA and subsequently diluted for virus titer determination by plaque assay (Figure 2B). As shown in Figure 2D, we found that addition of zinc chloride resulted in a significant reduction in the IAV titer. Previous research has shown that metal ions can destabilize viral proteins and we noted that the zinc chloride affected the pH of the incubation medium.[29] To gain more insights into the mechanism of virus inactivation, viral protein levels in the zinc chloride-treated samples were analyzed by western blot. As shown in Figure 2E, we found that in the presence of zinc chloride, soluble HA levels were reduced in a concentration-dependent manner, while NP levels did not diminish (Figure 2E). This result thus suggests that zinc ions may affect the IAV surface proteins more significantly than the internal proteins. To test if IAV RNA levels were affected, we added a 120-nucleotide long spike RNA to each sample, extracted viral RNA, and performed reverse transcriptions (RT) using a 3′ terminal NA primer. cDNA levels were next quantified using quantitative polymerase chain reaction (qPCR) of the NA gene-encoding segment and normalized to the spike RNA level (Figure 2E). No effect of zinc chloride on viral NA-encoding RNA segment levels was found. Together, these results imply that zinc ions can inactivate an IAV H1N1 strain by destabilization of the viral surface proteins.

Construction of a Fabric Containing Zinc Oxide. The above results suggest that zinc ions can directly inactivate an IAV H1N1 strain. To investigate if these inactivating properties are also present when zinc is embedded in a PA66 matrix (Figure 3A), we first prepared zinc-containing

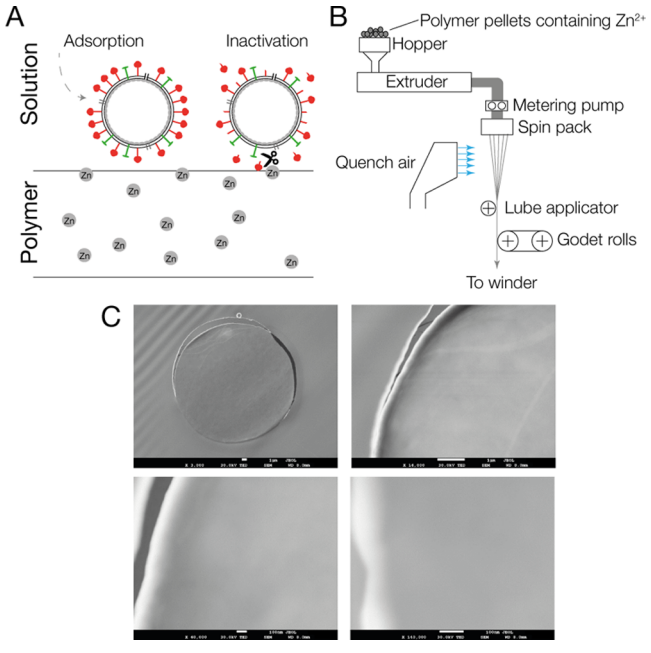

Figure 3. Construction of zinc-containing fabric. (A) Model for virus inactivation by zinc incorporated into fibers. A single PA66 unit is colored orange. (B) Schematic of a melt spinning operation to produce textile yarn. (C) SEM of zinc-containing fabric at 3,000×, 16,000×, 60,000×, and 140,000× magnification.

https://doi.org/10.1021/acsami.1c04412
ACS Appl. Mater. Interfaces 2021, 13, 30317−30325

PA66 polymer pellets by adding zinc ions from a zinc oxide source to the polymerization step. Next, the PA66 pellets were used to spin yarn (Figure 3B) and knit a single jersey fabric on a circular knitting machine. Scanning electron microscopy shows that no zinc oxide particles were visible in the polymer at 140,000× magnification (Figure 3C). The resulting fabrics, with internal code KF1, contained 328 ppm zinc ions and had an air permeability of 111 cfm/sq ft (Table 1). As a control, we also prepared a PA66 fabric that had similar characteristics but did not contain zinc (Table 1).

Table 1. Comparison of KF1 and Control Fabric

sample	Zn level (ppm)	basis weight (gsm)	thickness (mm)	air permeability (cfm/sq ft)	delta P per EN 14683 (mmH_2O/cm^2)
KF1	328	186	0.66	111	1.35
control	0	182	0.66	133	1.11

To investigate if fabrics constructed from fibers containing zinc maintain their zinc content after washing, we performed two experiments. In the first, 1 kg of fabric with 500 ppm zinc ions (equivalent to 5.3 mM; internal code KG6) was submerged into a wash solution (AATCC procedure 1-2018) and the wash water was retrieved after agitation. Next, the zinc content was measured using inductively coupled plasma (ICP) before and after capture of the zinc ion content using a cation exchange resin. We measured that only 0.149 ppm zinc was released from the fabric into the leachate and that all zinc content was captured by the exchange resin (Table 2). In our second experiment, we washed the fabric up to 50 times using the standardized home laundry test protocol AATCC M6-2016. Subsequent ICP-OES analysis of the zinc content in the fabric after washing revealed that the zinc content remained relatively stable in the PA66 fabrics during 50 washes (Table 3). Overall, these data suggest that the PA66 fibers contain mostly zinc ions and that these zinc ions are stably maintained in the fibers.

Table 2. Zinc Content in Leachate after Washing According to AATCC Test Protocol 1-2018 as Measured by ICP-OES[a]

leachate solution	Zn measured (ppm)
as prepared	0.149
stirred 30 min	below detection limit
stirred 60 min	below detection limit

[a]The leachate was exposed to cation exchange resin for 30 or 60 min under continuous stirring.

Influenza and Coronavirus Strains Are Inactivated on Fabrics Containing Zinc Ions. We next incubated 0.4 g of KF1 with virus and washed the fabrics using a PBS buffer containing 0.05% tween-80 and 10 mM EDTA (PBSTE; Figure 4A,B), which resulted in an approximately 2-log reduction of the IAV and SARS-CoV-2 titers compared to a PA66 control fabric after 1 h (Figure 4C,D). To confirm that inactivation of these viruses occurred on KF1, the viral protein levels were analyzed in the PBSTE wash eluate by western blot (Figure 4E,F). Any virus that remained in the fabric after extraction with PBSTE was lysed using Trizol and analyzed by western blot. Western blots showed a reduction in the soluble HA and S protein level in the virus eluate that was removed from the KF1 fabric compared to the control fabric eluate for IAV and SARS-CoV-2, respectively (Figure 4E,F). The signal obtained from the virus that remained on each fabric after the PBSTE extraction was close to background, in line with the observations in Figure 1. We were only able to quantify the SARS-CoV-2 signal but observed no statistically significant difference.

Table 3. Zinc Content in KG6 Fabric after Repeated Washing According to the Standardized Home Laundry Test Protocol AATCC M6-2016 as Measured by ICP-OES

no. of wash cycles	Zn level (ppm) after machine washes	Zn retention (%) in mask after machine washes
0	528	
10	518	98%
25	499	95%
50	505	96%

Overall, we conclude that inactivation of IAV and SARS-CoV-2 occurs on a fabric embedded with zinc oxide, analogous to the previously observed effects of cupric and cuprous oxide.[25,26,35] To better investigate the rate of reduction, we incubated KF1 with virus for different lengths of time and subtracted the adsorbed virus titer in the negative control from the level of reduction in the KF1 fabric and fitted the data with a logarithmic equation (Figure 4G). A maximum rate of virus titer reduction occurred between 30 s and 5 min of incubation, and the virus titer reduction reached a plateau after approximately 50 min.

Inactivation of IAV and Coronavirus Scales with Virus Load. To investigate the robustness and saturation level of the inactivation by fabrics containing embedded zinc oxide, we next performed experiments with KF1 and varied the viral load added to each fabric over a range of 10^3 to 10^7 pfu. The liquid volume applied to each fabric was kept constant. After incubation for different periods of time, fabrics were washed with PBSTE, and the virus titers were estimated by plaque assay. The virus titer reduction rate for the linear phase was subsequently calculated based on the shortest incubation time. Reduction rates were subsequently normalized by the dry weight of each fabric. As shown in Figure 4G, the rate of reduction in virus titer (in $pfu{\cdot}gram^{-1}{\cdot}min^{-1}$) scaled with virus load. On a log–log plot, the data could be fit with a linear equation. To confirm the robustness of these findings, we performed the same experiments with SARS-CoV-2 and found a similar behavior (Figure 4H).

Finally, we confirmed that the washed fabrics, which retained their zinc content after 50 washes (Table 3), were still able to reduce virus titers and incubated 0.4 g of unwashed or washed fabric with a fixed amount of IAV and removed inactivated virus with PBSTE. Analysis of the virus titers showed that both washed fabrics were able to reduce the IAV titer by approximately 2-logs (Figure 4I). Overall, these results suggest that the PA66 fabric containing zinc can inactivate both IAV and SARS-CoV-2 and that this property is retained after 50 washes. Given that zinc does not leach from the fibers, we suggest that both viruses are inactivated following adsorption to the solid fabric phase.

DISCUSSION

One way to fight RNA viruses is to limit respiratory virus spread through efficient PPE. To better understand how respiratory RNA viruses are adsorbed and inactivated on fabrics, we here added IAV and SARS-CoV-2 to cotton, PA66,

https://doi.org/10.1021/acsami.1c04412
ACS Appl. Mater. Interfaces 2021, 13, 30317−30325

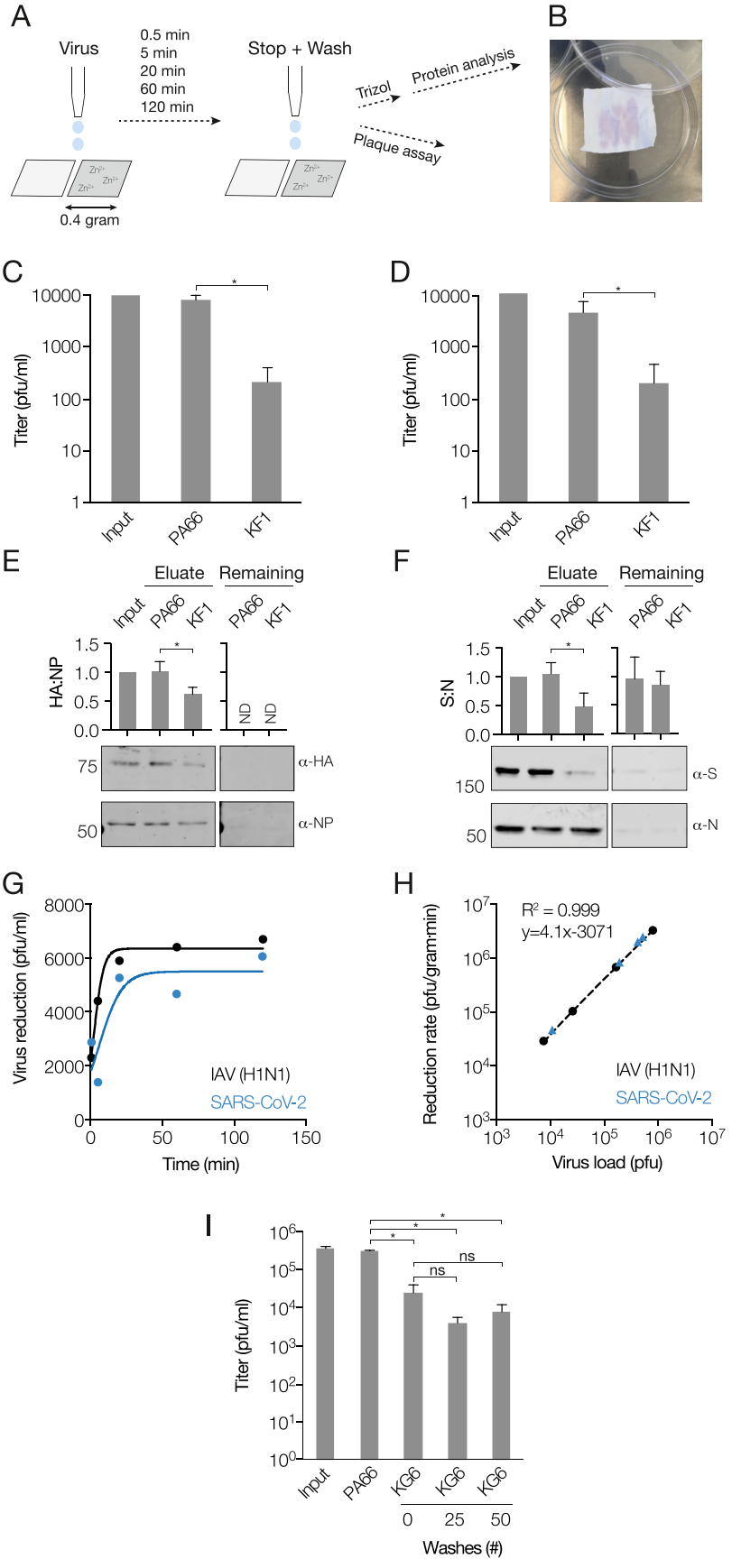

Figure 4. Inactivation of IAV and SARS-CoV-2 on fabrics. (A) Schematic of testing procedure for fabrics without or with embedded zinc oxide. (B) Photo of fabric placed in Petri dish and exposed to 100 μL sample (dyed red). (C) IAV titer in input or PA66 control or KF1 fabric eluates. (D) SARS-CoV-2 titer in input or PA66 control or KF1 fabric eluates. One representative experiment is shown. (E) Western blot analysis of IAV HA and NP protein levels after exposure of IAV to the KF1 or control fabric. Both the virus that was removed (eluate) from each fabric with PBSTE as

https://doi.org/10.1021/acsami.1c04412
ACS Appl. Mater. Interfaces 2021, 13, 30317−30325

Figure 4. continued

well as the virus that remained on each fabric was analyzed. (F) Western blot analysis of SARS-CoV-2 S and N protein levels after exposure of virus to the KF1 or control fabric. Both the virus that was removed (eluate) from each fabric with PBSTE as well as the virus that remained on each fabric was analyzed. G) Time course of IAV or SARS-CoV-2 titer reduction by the KF1 fabric minus the titer reduction by the PA66 control without embedded zinc. One representative time course is shown. Data were fit with logarithmic equation. (H) Reduction rate of IAV or SARS-CoV-2 titer after exposure to KF1 fabric. Data points were obtained by time course experiments in which we varied the viral load and subsequently estimated the maximum reduction rate (exponential phase) for each time course. Reduction was normalized to pfu·gram^{-1}·min^{-1} using the dry fabric weight. IAV and SARS-CoV-2 data points were fit with a linear line, and no difference was observed between the two fits. R^2 for IAV fit is shown. (I) Reduction rate of IAV titer after exposure to unwashed or washed KG6 fabric. Error bars represent standard deviation. Asterisk indicates p-value, with $^*p < 0.05$ and ns $p > 0.05$.

and PPP. We find strong liquid absorption by cotton and PA66 in PBS and that addition of tween-80 results in efficient virus release from PA66 but not from cotton. A previous clinical trial found that cotton masks with strong liquid absorbing properties may be associated with a higher risk of infection when reused and our finding that cotton does not release IAV or SARS-CoV-2 efficiently after washing is in line with this observation.[16] By contrast, virus retention on PPP, which is used for the construction of disposable 3-ply masks, is poor, in line with its hydrophobic properties.[34] This result implies that respiratory viruses remain on the surface of these masks, in line with findings that SARS-CoV-2 can survive up to 7 days on PPP-based surgical face masks.[19,36] However, PPP has important favorable properties, such as good breathability, filtration, and electrostatic properties and will thus have a purpose in the right situation.

Zinc and copper ions can inactivate IAV and SARS-CoV-2 (Figures 2, 4).[22,24,30] Using a zinc-containing PA66-based fabric from which we could easily remove adsorbed virus with a mild detergent (Figure 1), we consistently found a rapid reduction in the titer of both viruses and at viral loads that far exceed the number of infectious IAV particles present in a cough (Figure 4). After washing the fabrics using a standardized protocol, both the zinc content and the inactivating properties of the PA66 fabric were retained, suggesting that this fabric is reusable. This property may be of particular importance for designing reusable, "pathogen-free" PPE that could help reduce environmental waste, virus transmission, and costs.

We also investigated the mechanism by which zinc ions inactivate IAV and SARS-CoV-2. RT-qPCR analysis showed no significant reduction in viral RNA integrity after treatment with zinc ions. By contrast, analysis of the solubility of the viral surface and capsid proteins revealed a reduced level of the virus surface protein HA for IAV after exposure to zinc ions, while no effect on the internal nucleoprotein protein was detected. We observed a similar altered surface protein to nucleoprotein ratio after exposure to the zinc-containing PA66 fabric KF1. Together, these results suggest that the reduction in virus titer after exposure to zinc ions derives from inactivation of the viral surface proteins. This is in line with previous biochemical and electron microscopy studies showing the effect on divalent metals on viral protein stability and particle morphology.[29,37] Research has shown that zinc and copper ions can also induce oxidative reactions, inactivation of the viral proton channels, local pH changes, or viral membrane destabilization, and we cannot exclude that these processes may play a role in the inactivation as well.[31,38,39]

CONCLUSIONS

Overall, we show that zinc ions can inactivate IAV H1N1 and that a woven PA66 fabric containing zinc ions can decrease the IAV H1N1 and pandemic SARS-CoV-2 titer by approximately 2-logs. This reduction is more than sufficient to inactivate the number of infectious IAV particles (~24 pfu) present in a cough.[32] Overall, these results provide insights into the protective properties of fabrics and the development of testing protocols for reusable "pathogen-free" fabrics. Our findings may be important for healthcare workers who are exposed to infected patients for prolonged periods, people with underlying risk factors needing additional protection, and people who need to frequently remove their PPE.

METHODS

Influenza Viruses and Cells. HEK 293T and MDCK cells were originally sources from ATCC. Influenza A/WSN/33 (H1N1) virus was produced by transfecting a 12-plasmid rescue system into HEK 293T cells.[40] After 2 days, the P0 virus was amplified on MDCK cells in minimal essential medium (MEM) containing 0.5% fetal bovine serum (FBS) at 37 °C and 5% CO_2. P1 and P2 viruses were aliquoted and stored at −80 °C. For plaque assays, samples were serially diluted in MEM containing 0.5% FBS. Diluted virus (μL) was next added to confluent MDCK cells and incubated for 1 h 37 °C. After virus adsorption to the MDCK cells, the inoculum was removed and replaced with 2 mL of MEM/agarose overlay (MEM, 0.5% FBS, 1% low-melt agarose). Plaques were grown for 2 days at 37 °C and then fixed with 4% paraformaldehyde in PBS. Plaques were counter-stained with 0.01% crystal violet in water and washed with tap water before analysis.

Coronaviruses and Cells. SARS-CoV-2 (Bavpat-1 and USA-WA1/2020) was grown on African Green Monkey kidney epithelial Vero-E6 cells in Dulbecco's minimal essential medium (DMEM) supplemented with 10% FBS. For plaque assay analysis, Vero-E6 cells were seeded in 12-well plates and infected at 100% confluency. Ten-fold virus dilutions were grown under a 1% agarose overlay in DMEM containing 0.5% FBS for 2 days at 37 °C. Plaque assays were fixed with 4% paraformaldehyde in PBS and stained with 0.01% crystal violet in water. Experiments were performed in the Mt Sinai BSL3 lab according to the approved biosafety standards.

Cell Viability. To measure the effect of zinc ions or EDTA on the viability of the MDCK and Vero E6 cells used for plaque assays, we used a CellTiter Blue assay (Promega). Briefly, confluent cells were incubated with MEM containing 0.5% FBS and varying concentrations of zinc or EDTA. After 24 h, the medium was replaced with MEM containing 0.5% MEM and redox dye resazurin according to the manufacturer's instructions. Following conversion of resazurin to the fluorescent resofurin by viable cells, the fluorescent signal was measured using a 560 nm excitation wavelength and a 590 nm emission wavelength on a SpectraMax plate reader.

Construction of Zinc-Containing PA66 Fabrics. The PA66 fabrics were made from 70 denier 68 filament draw-textured PA66 yarn, which was spun from PA66 polymer-containing embedded zinc oxide (Microban Additive Zo7; EPA Reg. no. 42182-8). Zinc oxide (0.065% w/w) was brought into an ionic form and incorporated into

https://doi.org/10.1021/acsami.1c04412
ACS Appl. Mater. Interfaces 2021, 13, 30317−30325

the polymer pellets prior to the polymerization step. The polymer was made by Ascend Performance Materials in their facility in Pensacola, FL, and it was subsequently spun as a yarn, draw-textured into a bulk yarn, and then knitted on a circular knitting machine into a single jersey fabric. The KF-1 fabric was dyed with Lanasyn Black S-DL-C p 120 (Anchroma USA, Inc) according to the manufacturer's instructions. The control and other fabrics tested were not dyed.

Washing and Zinc Content Analysis. For analysis of the zinc release from the PA66 fabric, 1 kg of fabric containing 500 ppm zinc was washed according to AATCC lab procedure 1-2018. After the agitation cycle, a leachate sample was analyzed using ICP-OES to measure the zinc content. Next, 50 g of leachate was mixed with 1 g of cation exchange resin Lewatit TP 260 in H^+ form and the remaining zinc content of the supernatant measured using ICP-OES after 30 min. For analysis of zinc release following repeated washing, PA66 fabrics were washed according to the standardized home laundry test protocol AATCC M6-2016. The zinc content in fabric samples was analyzed by ICP-OES analysis. To test if zinc oxide had affected the polymerization and yarn production process or whether zinc oxide particles were present in the fibers, fabric samples with a thickness of ~0.5 μm were taken using a Reichert Jung Ultramicrotome. Samples were analyzed by SEM/TED at 30.0 kV at different magnifications.

Other Fabrics. The cotton fabric was issued and certified by the IAC (lot number IACVC01012020). The PPP disposable type II 3-ply face mask (Medical Products Co, Ltd) was BS EN14638:2019 type II compliant.

Virus Adsorption and Extraction. Fabrics were stored at room temperature in sealed plastic bags. Prior to each experiment, fabric samples were cut to size using scissors sterilized with 75% ethanol. The size of the fabrics varied from 1 cm^2 to 0.4 g, as indicated in the figures. To test the ability of fabrics to reduce viral titers, we used a modified ISO 18184 protocol. Briefly, 100 μL of IAV strain A/WSN/33 (H1N1) was carefully applied to fabrics in 2−10 μL droplets that were spread over each fabric in a serpentine pattern. After incubation at room temperature as indicated, the fabrics were placed in 50 mL tubes containing 900 μL of PBS, PBS containing different percentages tween-80, or PBS containing 0.05% tween-80 and 10 mM EDTA. Fabrics were washed by vortexing them inside the 50 mL tubes for approximately 1 min. After centrifugation, all liquid was squeezed from each fabric and the 1 cm fabrics transferred to an Eppendorf tube containing 1 mL of Trizol (Invitrogen) to extract remaining viral protein and RNA. Experiments were performed in triplicate, unless noted otherwise. Data was analyzed in Graphpad Prism 8 using 1-way ANOVA.

RT-qPCR and Western Blot. RNA extraction from Trizol was performed as described previously,[41] while protein was extracted from the interphase using isopropanol precipitation.[42] The precipitated protein was washed in ethanol, resuspended in 5× SDS-PAGE loading buffer, sonicated for 10 s, and boiled for 10 min before 8% SDS-PAGE analysis. Western blot was performed using antibodies directed against IAV HA (Invitrogen, PA5-34929) and NP (GeneTex, GTX125989) and SARS-CoV-2 S (Abcam ab272504) and N (GeneTex, GTX632269). Membranes were washed in TBS containing 0.1% tween-20. Spike RNA was purchased from IDT and had the sequence 5′-AGUAGAAACAAGGCGGUAGGCGCUGUCCUUUAUCCAGACAACCAUUACCUGUCCACACAAUCUGCCCUUUCGAAAGAUCCCAACGAAAAGAGAGACCACAUGGUCCUUCCUGCUUUUGCU-3′. Isolated RNA was reverse-transcribed using SuperScript III and a primer binding to the 3′ end of the NA segment.[41] qPCR was performed as described previously.[41] Data was analyzed in Graphpad Prism 8 using one-way ANOVA with multiple corrections.

AUTHOR INFORMATION

Corresponding Authors

Vikram Gopal − *Ascend Performance Materials, Houston, Texas 77002, United States*; Email: VGopal@ascendmaterials.com

Aartjan J. W. te Velthuis − *Division of Virology, Department of Pathology, Addenbrooke's Hospital, University of Cambridge, Cambridge CB2 2QQ, U.K.*; Present Address: Lewis Thomas Laboratory, Department of Molecular Biology, Princeton University.; orcid.org/0000-0002-5129-3953; Email: ajwt6@cam.ac.uk

Authors

Benjamin E. Nilsson-Payant − *Department of Microbiology, Icahn School of Medicine at Mount Sinai, New York 10029, United States*

Hollie French − *Division of Virology, Department of Pathology, Addenbrooke's Hospital, University of Cambridge, Cambridge CB2 2QQ, U.K.*

Jurre Y. Siegers − *Department of Viroscience, Erasmus University Medical Centre, Rotterdam 3015 GD, the Netherlands*

Wai-shing Yung − *Ascend Performance Materials, Houston, Texas 77002, United States*

Matthew Hardwick − *ResInnova Laboratories, Silver Spring, Maryland 20910, United States*

Complete contact information is available at: https://pubs.acs.org/10.1021/acsami.1c04412

Funding

This study was funded in part by Ascend Performance Materials. AtV is supported by joint Wellcome Trust and Royal Society grant 206579/Z/17/Z.

Notes

The authors declare the following competing financial interest(s): This study was funded in part by Ascend Performance Materials. VG and W-sY are employed by Ascend Performance Materials. MH is employed by ResInnova and hired by Ascend Performance Materials to perform experiments and analyze data. Icahn School of Medicine at Mount Sinai and University of Cambridge received consultancy fees from Ascend Performance Materials for experimental work and data analysis.

ACKNOWLEDGMENTS

We thank Shanaka Rodrigo, Natasha Virjee, Chris Hsiung, and Benjamin tenOever for helpful discussions, support, materials, and information.

REFERENCES

(1) Vieira, J. M.; Ricardo, O. M. P.; Hannas, C. M.; Kanadani, T. C. M.; Prata, T. D. S.; Kanadani, F. N. What do we know about COVID-19? A review article. *Rev. Assoc. Med. Bras.* **2020**, *66*, 534−540.

(2) Hutchinson, E. C.; Charles, P. D.; Hester, S. S.; Thomas, B.; Trudgian, D.; Martínez-Alonso, M.; Fodor, E. Conserved and host-specific features of influenza virion architecture. *Nat. Commun.* **2014**, *5*, 4816.

(3) Te Velthuis, A. J. W.; Fodor, E. Influenza virus RNA polymerase: insights into the mechanisms of viral RNA synthesis. *Nat. Rev. Microbiol.* **2016**, *14*, 479−493.

(4) Zhu, N.; Zhang, D.; Wang, W.; Li, X.; Yang, B.; Song, J.; Zhao, X.; Huang, B.; Shi, W.; Lu, R.; Niu, P.; Zhan, F.; Ma, X.; Wang, D.; Xu, W.; Wu, G.; Gao, G. F.; Tan, W.; China Novel Coronavirus, I.; Research, T. A Novel Coronavirus from Patients with Pneumonia in China, 2019. *N. Engl. J. Med.* **2020**, *382*, 727−733.

(5) Coronaviridae Study Group of the International Committee on Taxonomy of Viruses. The species Severe acute respiratory syndrome-related coronavirus: classifying 2019-nCoV and naming it SARS-CoV-2. *Nat. Microbiol.* **2020**, *5*, 536−544.

(6) Letko, M.; Marzi, A.; Munster, V. Functional assessment of cell entry and receptor usage for SARS-CoV-2 and other lineage B betacoronaviruses. *Nat. Microbiol.* **2020**, *5*, 562−569.
(7) Goldhill, D. H.; Te Velthuis, A. J. W.; Fletcher, R. A.; Langat, P.; Zambon, M.; Lackenby, A.; Barclay, W. S. The mechanism of resistance to favipiravir in influenza. *Proc. Natl. Acad. Sci. U. S. A.* **2018**, *115*, 11613−11618.
(8) Pruijssers, A. J.; George, A. S.; Schäfer, A.; Leist, S. R.; Gralinksi, L. E.; Dinnon, K. H., 3rd; Yount, B. L.; Agostini, M. L.; Stevens, L. J.; Chappell, J. D.; Lu, X.; Hughes, T. M.; Gully, K.; Martinez, D. R.; Brown, A. J.; Graham, R. L.; Perry, J. K.; Du Pont, V.; Pitts, J.; Ma, B.; Babusis, D.; Murakami, E.; Feng, J. Y.; Bilello, J. P.; Porter, D. P.; Cihlar, T.; Baric, R. S.; Denison, M. R.; Sheahan, T. P. Remdesivir Inhibits SARS-CoV-2 in Human Lung Cells and Chimeric SARS-CoV Expressing the SARS-CoV-2 RNA Polymerase in Mice. *Cell Rep.* **2020**, *32*, 107940.
(9) Williamson, B. N.; Feldmann, F.; Schwarz, B.; Meade-White, K.; Porter, D. P.; Schulz, J.; van Doremalen, N.; Leighton, I.; Yinda, C. K.; Pérez-Pérez, L.; Okumura, A.; Lovaglio, J.; Hanley, P. W.; Saturday, G.; Bosio, C. M.; Anzick, S.; Barbian, K.; Cihlar, T.; Martens, C.; Scott, D. P.; Munster, V. J.; de Wit, E. Clinical benefit of remdesivir in rhesus macaques infected with SARS-CoV-2. *Nature* **2020**, *585*, 273−276.
(10) van Riel, D.; de Wit, E. Next-generation vaccine platforms for COVID-19. *Nat. Mater.* **2020**, *19*, 810−812.
(11) Eckerle, L. D.; Becker, M. M.; Halpin, R. A.; Li, K.; Venter, E.; Lu, X.; Scherbakova, S.; Graham, R. L.; Baric, R. S.; Stockwell, T. B.; Spiro, D. J.; Denison, M. R. Infidelity of SARS-CoV Nsp14-exonuclease mutant virus replication is revealed by complete genome sequencing. *PLoS Pathog.* **2010**, *6*, No. e1000896.
(12) Cheung, P. P.-H.; Rogozin, I. B.; Choy, K.-T.; Ng, H. Y.; Peiris, J. S. M.; Yen, H.-L. Comparative mutational analyses of influenza A viruses. *RNA* **2015**, *21*, 36−47.
(13) Gandhi, M.; Beyrer, C.; Goosby, E. Masks Do More Than Protect Others During COVID-19: Reducing the Inoculum of SARS-CoV-2 to Protect the Wearer. *J. Gen. Intern. Med.* **2020**, *35*, 3063.
(14) Jefferson, T.; Del Mar, C. B.; Dooley, L.; Ferroni, E.; Al-Ansary, L. A.; Bawazeer, G. A.; van Driel, M. L.; Nair, S.; Jones, M. A.; Thorning, S.; Conly, J. M. Physical interventions to interrupt or reduce the spread of respiratory viruses. *Cochrane Database Syst. Rev.* **2011**, *7*, CD006207.
(15) Wu, J.; Xu, F.; Zhou, W.; Feikin, D. R.; Lin, C.-Y.; He, X.; Zhu, Z.; Liang, W.; Chin, D. P.; Schuchat, A. Risk factors for SARS among persons without known contact with SARS patients, Beijing, China. *Emerg. Infect. Dis.* **2004**, *10*, 210−216.
(16) MacIntyre, C. R.; Seale, H.; Dung, T. C.; Hien, N. T.; Nga, P. T.; Chughtai, A. A.; Rahman, B.; Dwyer, D. E.; Wang, Q. A cluster randomised trial of cloth masks compared with medical masks in healthcare workers. *BMJ Open* **2015**, *5*, No. e006577.
(17) Wang, Y.; Tian, H.; Zhang, L.; Zhang, M.; Guo, D.; Wu, W.; Zhang, X.; Kan, G. L.; Jia, L.; Huo, D.; Liu, B.; Wang, X.; Sun, Y.; Wang, Q.; Yang, P.; MacIntyre, C. R. Reduction of secondary transmission of SARS-CoV-2 in households by face mask use, disinfection and social distancing: a cohort study in Beijing, China. *BMJ Glob Health* **2020**, *5*, No. e002794.
(18) Fischer, R. J.; Morris, D. H.; van Doremalen, N.; Sarchette, S.; Matson, M. J.; Bushmaker, T.; Yinda, C. K.; Seifert, S. N.; Gamble, A.; Williamson, B. N.; Judson, S. D.; de Wit, E.; Lloyd-Smith, J. O.; Munster, V. J. Effectiveness of N95 Respirator Decontamination and Reuse against SARS-CoV-2 Virus. *Emerg. Infect. Dis.* **2020**, *26*, 2253.
(19) Chin, A. W. H.; Chu, J. T. S.; Perera, M. R. A.; Hui, K. P. Y.; Yen, H.-L.; Chan, M. C. W.; Peiris, M.; Poon, L. L. M. Stability of SARS-CoV-2 in different environmental conditions − Authors' reply. *Lancet Microbe* **2020**, *1*, No. e146.
(20) Prata, J. C.; Silva, A. L. P.; Walker, T. R.; Duarte, A. C.; Rocha-Santos, T. COVID-19 Pandemic Repercussions on the Use and Management of Plastics. *Environ. Sci. Technol.* **2020**, *54*, 7760−7765.
(21) Adyel, T. M. Accumulation of plastic waste during COVID-19. *Science* **2020**, *369*, 1314−1315.
(22) Noyce, J. O.; Michels, H.; Keevil, C. W. Inactivation of influenza A virus on copper versus stainless steel surfaces. *Appl. Environ. Microbiol.* **2007**, *73*, 2748−2750.
(23) Biryukov, J.; Boydston, J. A.; Dunning, R. A.; Yeager, J. J.; Wood, S.; Reese, A. L.; Ferris, A.; Miller, D.; Weaver, W.; Zeitouni, N. E.; Phillips, A.; Freeburger, D.; Hooper, I.; Ratnesar-Shumate, S.; Yolitz, J.; Krause, M.; Williams, G.; Dawson, D. G.; Herzog, A.; Dabisch, P.; Wahl, V.; Hevey, M. C.; Altamura, L. A. Increasing Temperature and Relative Humidity Accelerates Inactivation of SARS-CoV-2 on Surfaces. *mSphere* **2020**, *5*, No. e00441.
(24) Warnes, S. L.; Little, Z. R.; Keevil, C. W. Human Coronavirus 229E Remains Infectious on Common Touch Surface Materials. *mBio* **2015**, *6*, No. e01697.
(25) Hosseini, M.; Chin, A. W. H.; Behzadinasab, S.; Poon, L. L. M.; Ducker, W. A. Cupric Oxide Coating That Rapidly Reduces Infection by SARS-CoV-2 via Solids. *ACS Appl. Mater. Interfaces* **2021**, *13*, 5919−5928.
(26) Behzadinasab, S.; Chin, A.; Hosseini, M.; Poon, L.; Ducker, W. A. A Surface Coating that Rapidly Inactivates SARS-CoV-2. *ACS Appl. Mater. Interfaces* **2020**, *12*, 34723−34727.
(27) Sousa, B. C.; Cote, D. L. Antimicrobial Copper Cold Spray Coatings and SARS-CoV-2 Surface Inactivation. *MRS Adv.* **2020**, *5*, 2873−2880.
(28) Jeremiah, S. S.; Miyakawa, K.; Morita, T.; Yamaoka, Y.; Ryo, A. Potent antiviral effect of silver nanoparticles on SARS-CoV-2. *Biochem. Biophys. Res. Commun.* **2020**, *533*, 195−200.
(29) Fujimori, Y.; Sato, T.; Hayata, T.; Nagao, T.; Nakayama, M.; Nakayama, T.; Sugamata, R.; Suzuki, K. Novel antiviral characteristics of nanosized copper(I) iodide particles showing inactivation activity against 2009 pandemic H1N1 influenza virus. *Appl. Environ. Microbiol.* **2012**, *78*, 951−955.
(30) Imai, K.; Ogawa, H.; Bui, V. N.; Inoue, H.; Fukuda, J.; Ohba, M.; Yamamoto, Y.; Nakamura, K. Inactivation of high and low pathogenic avian influenza virus H5 subtypes by copper ions incorporated in zeolite-textile materials. *Antiviral Res.* **2012**, *93*, 225−233.
(31) Binder, H.; Arnold, K.; Ulrich, A. S.; Zschörnig, O. Interaction of Zn2+ with phospholipid membranes. *Biophys. Chem.* **2001**, *90*, 57−74.
(32) Lindsley, W. G.; Noti, J. D.; Blachere, F. M.; Thewlis, R. E.; Martin, S. B.; Othumpangat, S.; Noorbakhsh, B.; Goldsmith, W. T.; Vishnu, A.; Palmer, J. E.; Clark, K. E.; Beezhold, D. H. Viable influenza A virus in airborne particles from human coughs. *J. Occup. Environ. Hyg.* **2015**, *12*, 107−113.
(33) Cruz, J.; Leitão, A.; Silveira, D.; Pichandi, S.; Pinto, M.; Fangueiro, R. Study of moisture absorption characteristics of cotton terry towel fabrics. *Procedia Eng.* **2017**, *200*, 389−398.
(34) Erbil, H. Y.; Demirel, A. L.; Avci, Y.; Mert, O. Transformation of a simple plastic into a superhydrophobic surface. *Science* **2003**, *299*, 1377−1380.
(35) Borkow, G.; Zhou, S. S.; Page, T.; Gabbay, J. A novel anti-influenza copper oxide containing respiratory face mask. *PLoS One* **2010**, *5*, No. e11295.
(36) van Doremalen, N.; Bushmaker, T.; Morris, D. H.; Holbrook, M. G.; Gamble, A.; Williamson, B. N.; Tamin, A.; Harcourt, J. L.; Thornburg, N. J.; Gerber, S. I.; Lloyd-Smith, J. O.; de Wit, E.; Munster, V. J. Aerosol and Surface Stability of SARS-CoV-2 as Compared with SARS-CoV-1. *N. Engl. J. Med.* **2020**, *382*, 1564−1567.
(37) Escors, D.; Ortego, J.; Laude, H.; Enjuanes, L. The membrane M protein carboxy terminus binds to transmissible gastroenteritis coronavirus core and contributes to core stability. *J. Virol.* **2001**, *75*, 1312−1324.
(38) Gandhi, C. S.; Shuck, K.; Lear, J. D.; Dieckmann, G. R.; DeGrado, W. F.; Lamb, R. A.; Pinto, L. H. Cu(II) inhibition of the proton translocation machinery of the influenza A virus M2 protein. *J. Biol. Chem.* **1999**, *274*, 5474−5482.
(39) Okada, A.; Miura, T.; Takeuchi, H. Zinc- and pH-Dependent Conformational Transition in a Putative Interdomain Linker Region

https://doi.org/10.1021/acsami.1c04412
ACS Appl. Mater. Interfaces 2021, 13, 30317−30325

of the Influenza Virus Matrix Protein M1†. *Biochemistry* **2003**, *42*, 1978−1984.
(40) Fodor, E.; Devenish, L.; Engelhardt, O. G.; Palese, P.; Brownlee, G. G.; García-Sastre, A. Rescue of Influenza A Virus from Recombinant DNA. *J. Virol.* **1999**, *73*, 9679−9682.
(41) Te Velthuis, A. J. W.; Long, J. C.; Bauer, D. L. V.; Fan, R. L. Y.; Yen, H.-L.; Sharps, J.; Siegers, J. Y.; Killip, M. J.; French, H.; Oliva-Martín, M. J.; Randall, R. E.; de Wit, E.; van Riel, D.; Poon, L. L. M.; Fodor, E. Mini viral RNAs act as innate immune agonists during influenza virus infection. *Nat. Microbiol.* **2018**, *3*, 1234−1242.
(42) Simões, A. E.; Pereira, D. M.; Amaral, J. D.; Nunes, A. F.; Gomes, S. E.; Rodrigues, P. M.; Lo, A. C.; D'Hooge, R.; Steer, C. J.; Thibodeau, S. N.; Borralho, P. M.; Rodrigues, C. M. Efficient recovery of proteins from multiple source samples after trizol or trizolLS RNA extraction and long-term storage. *BMC Genomics* **2013**, *14*, 181.

https://doi.org/10.1021/acsami.1c04412
ACS Appl. Mater. Interfaces 2021, 13, 30317−30325